 MCB, vol.4, no.4, pp.211-226, 2007

In Vitro Measurement and Calculation of Drag Force on Iliac Limb Stentgraft in a Compliant Arterial Wall Model

A. Sinha Roy*, K. West†, R. S. Rontala[1], R. K. Greenberg[2] and R. K. Banerjee[1,‡]

Abstract: Interventional treatment of aortic aneurysms using endovascular stentgrafting is a minimally invasive technique. Following device implantation, transient drag forces act on the stentgraft. When the drag force exceeds the fixation force, complications like stentgraft migration, endoleaks and stentgraft failure occur. In such a scenario the device becomes unstable, causing concern over the long-term durability of endovascular repairs. The objective of this study is: 1) to measure the drag force on iliac limb stentgraft, having a distal diameter that is half the size of the proximal end, in an *in vitro* experiment; 2) to calculate the drag force using blood flow–compliant arterial wall interaction model and compare it with the measured values on the stentgraft for the *in vitro* experiment; 3) to calculate drag force on the stentgraft using physiological flow conditions. Experimental data for a stentgraft within a silicon tubing, representing a compliant artery, shows a peak drag force of 2.79 N whereas the calculation predicts a peak drag force of 2.57 N; thus a percentage difference of 7.8 % is observed. When physiological flow and pressure pulse are used for the blood flow-compliant arterial wall computations, a peak drag force of 0.59 N is obtained for the same stentgraft that was used in the experiment. The outer cavity between the distal end of the iliac limb stentgraft and the arterial wall reduces the drag force. These forces can be used as design guideline for determining the fixation force needed for the stentgraft under physiological pulsatile flow.

Keyword: Endovascular grafting; Abdominal aortic aneurysm; Drag force; Compliant arterial wall; Pulsatile blood flow

1 Introduction

An aneurysm is the dilation of a weakened vessel. If left untreated, the aneurysm could expand and rupture. Aortic aneurysms (AA) are common and represent the 10^{th} leading cause of death in white males over 55 years of age. According to a recent study [1], the prevalence of AA is 8.8 % in population above 65 years. Endovascular aneurysm repair is a minimally invasive interventional technique where the diseased aorta is replaced by a stentgraft. During this procedure, the endovascular graft (EVG) or the stentgraft is guided to the affected site through the femoral artery into the iliac artery and then to aorta where it is expanded to shield the aneurysm wall from the hemodynamic forces caused by the pulsatile blood flow. Endovascular grafting (EVG), an alternative to open surgery procedure, has become successful due to a reduction in pre-operative procedures, mortality and morbidity [2-4]. However, late complications such as stentgraft migration, endoleaks and device integrity failure still occur [5,6]. Migration in particular, raises concern over the long term stability of such a device in the context of challenging hemodynamic conditions [7]. The causes of migration relate to the drag force imparted to the stentgraft by the pulsatile blood flow or extension of the aneurysm into the region of the aorta used to fix the stentgraft. The later is minimized by proper preoperative imaging and selection of

* Department of Mechanical Engineering, University of Cincinnati, Cincinnati, OH 45221, USA.

† The Endovascular Branch vessel laboratory, Cleveland Clinic Foundation, Cleveland, OH 44195, USA.

‡ Corresponding Author. Dept. of Mechanical, Industrial and Nuclear Engineering, 688 Rhodes Hall, PO Box 210072, Cincinnati OH, 45221 0072, Tel: 513-556-2124, Fax: 513 556-3390, Email: Rupak.Banerjee@UC.edu. The first, second and third authors contribute equally to this manuscript.

location while the former requires a durable device design capable of resisting the applied drag force. Thus, when the drag force exceeds the fixation force, the device becomes unstable.

Recently, studies have analyzed the effect of hemodynamics on a stentgraft. The studies have shown that increase in proximal stentgraft to iliac limb diameter ratio increases the drag force [8-11]. A mathematical model to predict the *in vivo* pulsatile drag force acting on a bifurcated stentgraft without considering the outer stagnant blood cavity has been analyzed and has shown that an increase in proximal diameter of the stentgraft and compliance of the aorta increases the drag force [12]. Both analytical and numerical evaluation of the drag force on a bifurcated stentgraft has been performed and the study shows that the proximal diameter of the stentgraft plays an important role on the net force acting on the stentgraft [13]. In another study, a quantitative local evaluation of the stresses due to local structural and fluid dynamic conditions has been provided using blood flow-arterial wall interaction of a three dimensional aneurysm model obtained from computed tomography (CT) scan images [14].

A previous study has reported experimental work using an *in vitro* model to visualize the flow patterns in different commercially available stentgrafts to understand the hemodynamics [15]. Flow visualization results have indicated that there are no significant changes in the flow patterns between an exo-stent (where the stent is affixed to the outside of the graft) and endo-stent (where the stent is mounted within the graft) configuration. An *in vitro* experiment on vascular graft has been performed and has concluded that very low displacement force is required when the pressure in the aneurysm sac is equal to the systemic pressure [16]. Longitudinal force required to cause migration of a stentgraft in a human cadaveric aorta has also been studied [17]. Stents with hooks and barbs tend to increase the fixation of the stentgrafts tenfold, while the radial force has minimal impact [18]. Lawerence and colleagues [19] have analyzed different attachment patterns for the stentgraft at the proximal end in an *in vitro* model and concluded that contoured (zigzag) attachments of graft material to the stents reduces the fixation force. Resch and colleagues [20, 21] have performed experiments with cadaveric aorta to obtain the fixation force for different commercially available stentgrafts and reported that dilation in the proximal neck region is the main cause for the migration of the stentgraft.

From figure 1A, it can be seen that the proximal end of the stentgraft before the bifurcation has limited scope of any design improvements because the diameter is sized to optimize fixation and sealing to prevent failure due to endoleaks as evidenced clinically. However, there is a possibility of reduction in the overall drag on the entire bifurcated stentgraft by reducing the diameter of the free (unanchored) distal end of the iliac limb segment. Thus, there are two possible cases for the iliac limb stentgraft segment: (1) the distal end of the iliac limb of stentgraft has a diameter smaller than its proximal end, such that only the proximal end is anchored and there is a cavity between the stentgraft and arterial wall (see figure 1A, left limb); (2) the proximal and distal end of the iliac limb stentgraft have the same diameter and both ends are anchored such that the stentgraft is flushed to the arterial wall (see figure 1A, right limb). Thus, case 1 is similar to case 2 except for the reduced distal diameter of the iliac limb stentgraft.

In figure 1A, the right limb shows the case 2 of the iliac limb segment of the stentgraft whereas the left bifurcation shows the proposed case 1. One of the main causes of stentgraft failure is underestimation of the hemodynamic forces placed on the stentgraft's fixation sites. These types of failures will re-pressurize the aneurysm sac and increasing the probability of rupture. In figure 1A, the top X-ray image illustrates an iliac limb segment properly mated with an AAA device and its distal end anchored to the distal artery, having the same diameter as its proximal end; the arrow indicates the overlapping segment. Due to elevated displacement forces caused by the large angle and pulsatility of the blood flow within the extension device, the iliac limb segment separates from its host; see bottom X-ray image in figure 1A. This type of failure will require additional surgical in-

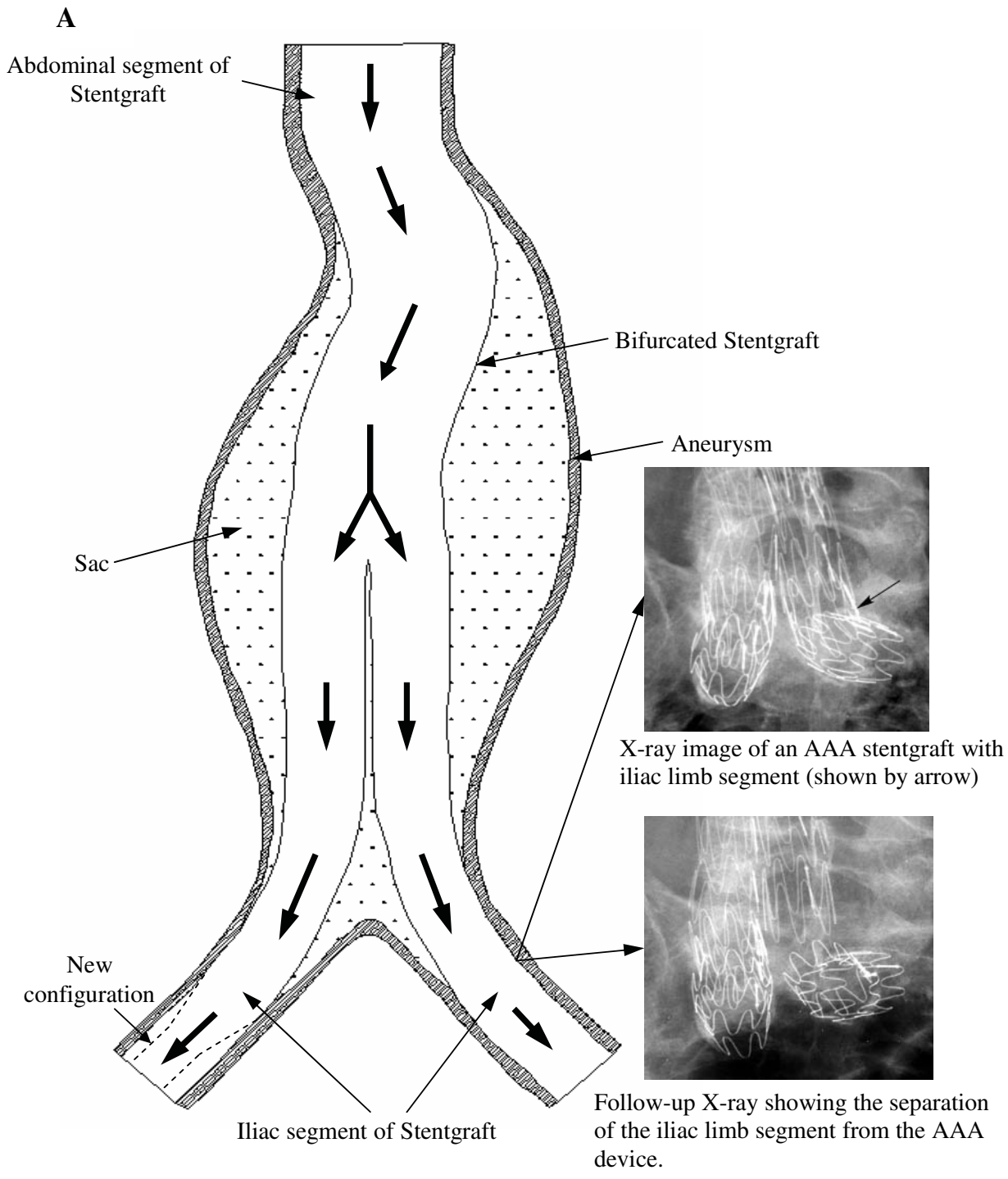
A
Abdominal segment of Stentgraft
Bifurcated Stentgraft
Aneurysm
Sac
X-ray image of an AAA stentgraft with iliac limb segment (shown by arrow)
New configuration
Iliac segment of Stentgraft
Follow-up X-ray showing the separation of the iliac limb segment from the AAA device.

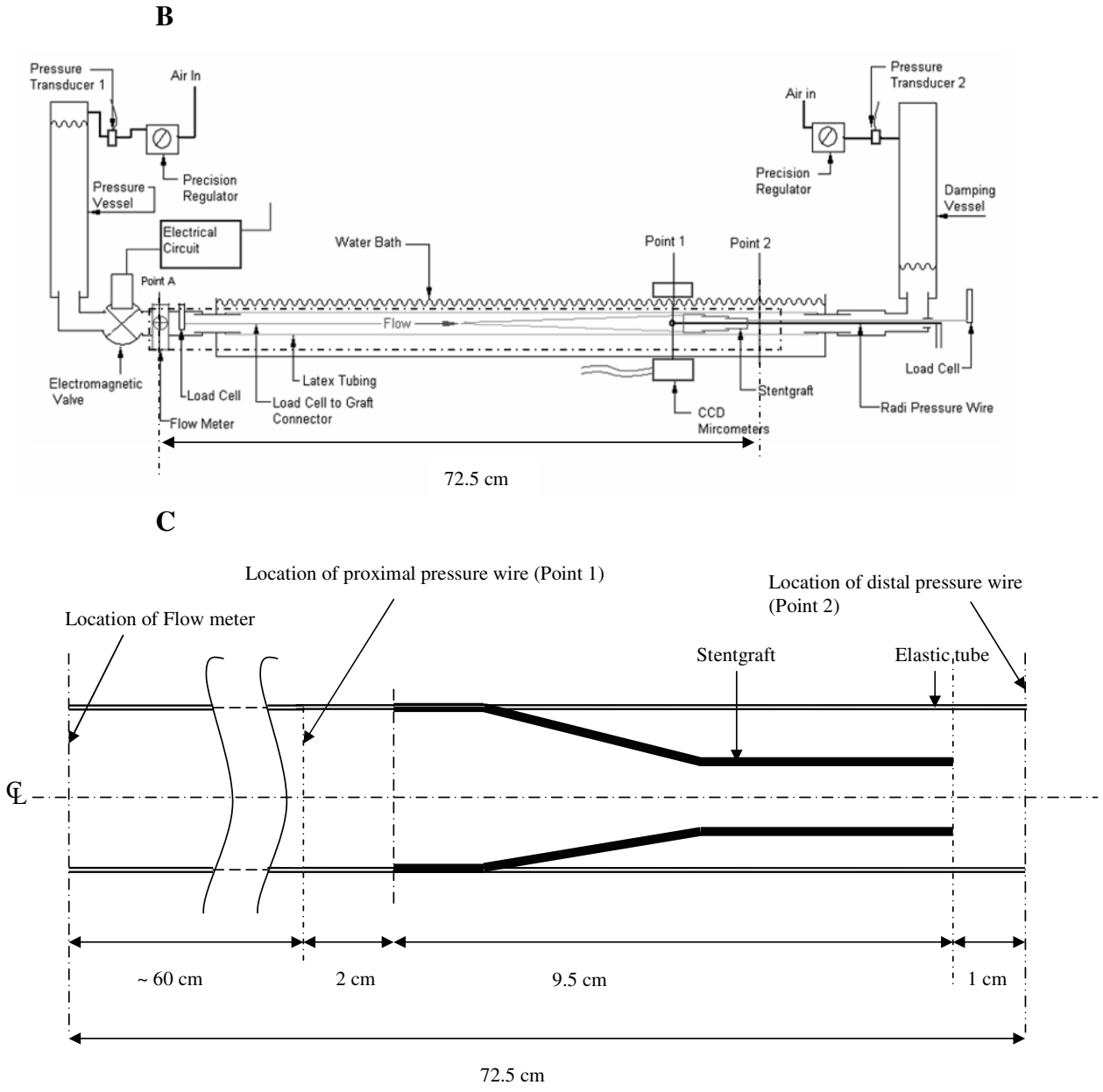

Figure 1: A. Schematic diagram of the stentgraft. The left bifurcation shows the proposed iliac limb stentgraft, having a distal diameter that is half the size of the proximal end, and an earlier design where the inlet and outlet diameters of the iliac stentgraft are the same (right bifurcation); B. Schematic representation of the *in vitro* set up for the evaluation of drag force; C. Location of the pressure and flow probes.

tervention and will be repaired by inserting an additional stentgraft device to gap the separation. Thus, the case 2 is prone to failure in patients and is clinically less relevant. Hence, this case has not been evaluated further.

In this study, an iliac limb section of the Zenith® Renu™ AAA ancillary graft (Cook Incorporated, IN) has been investigated by *in vitro* and computational methods. The objective of this study is to measure the peak drag force on an iliac limb section of the stentgraft in an *in vitro* experiment and validate the results using a blood flow–compliant arterial wall analysis of the stentgraft model used in the *in vitro* experiment. Thus, for case 1, the blood pressure in the cavity between the distal iliac artery and the distal end of the stentgraft will apply a stabilizing force on the stentgraft (see left limb in figure 1A). This stabilizing force will not exist in case 2. Thus, leaving the outlet of the iliac limb stengraft free could significantly reduce the failure rates. In comparison with past studies, the drag force has been measured by using an *in vitro* model representing a compliant artery and subsequently validated using computational means. An improvement to reduce the net drag force on iliac limb stentgraft has been suggested based on inferences obtained from experiment and computational model.

2 Methods

2.1 Experimental set up

The *in vitro* experiment has been conducted by the Endovascular Branch Vessel Laboratory at the Cleveland Clinic. Fig. 1B shows the schematic representation of the single pulse wave elastic tube *in vitro* model. The *in vitro* set up consists of a stentgraft radially secured within an elastic tube immersed in a water bath. A transonic flow probe positioned 60 cm proximally to the stentgraft measures the fluid velocity. Two internal pressure guide wires of diameter 0.014 inch (Radi Medical systems, MA) are used to obtain the pressure 2 cm proximal and 1 cm distal to the stentgraft. The stentgraft is an iliac limb of a Zenith AAA (Cook, Bloomington, IN) endovascular graft with an exo-stent configuration, where the stainless steel stents are fixed outside to the graft. Fig. 1C shows the geometry of the stentgraft with the location of the flow probe and pressure wires. The elastic tube is immersed in the water bath to eliminate the effect of contact stresses between the elastic tube and bath surface.

The *in vitro* model has been developed to simulate the forces that would be encountered by the proposed model of iliac limb stentgraft in actual physiological conditions. Since the stentgraft used for this study is an iliac limb of an AAA graft, only a straight artery model is considered rather than a bulging aneurysm model [8-11]. The elastic tubing is an elastomer (Sylgard 184, Dow corning, Midland, MI), with the stentgraft radially fixed on its inner wall. By activating an electromagnetic valve for approximately 80 ms and maintaining a pressure differential of 150 mm Hg between two reservoirs generates a single pulse wave. The test fluid used in the *in vitro* experiment is water having properties:μ = 0.01 Poise and ρ= 1 gm/cm^3. Ten thousand data points for each of the observed variables, the pressure (proximal and distal), inlet velocity and stentgraft displacement forces were collected for a cycle time of 1.25 sec subsequent to the valve activation. The velocity data is acquired proximal to the stentgraft at point A (Fig. 1B). Pressure waveforms are measured at points 1 and 2 of the stentgraft (Fig. 1B). The force acting on the proximal end of the stentgraft is measured by a calibrated beam load cell (Transducer Techniques, CA). The data of interest is the peak drag force acting on the stentgraft model. The peak inlet pressure and flow generated in the *in vitro* experiment are 140 mm Hg and 75 cm/s, respectively. The data from sensors are recorded by a data acquisition system (LabView 7.1) integrated to a computer.

3 Blood flow - Compliant artery wall Interaction Model using Fluid Structure Interaction (FSI) Technique

3.1 Geometry

Fig. 2A shows the axi-symmetric model of the stentgraft along with the pulsatile fluid flow domain and cavity region in between the elastic tube

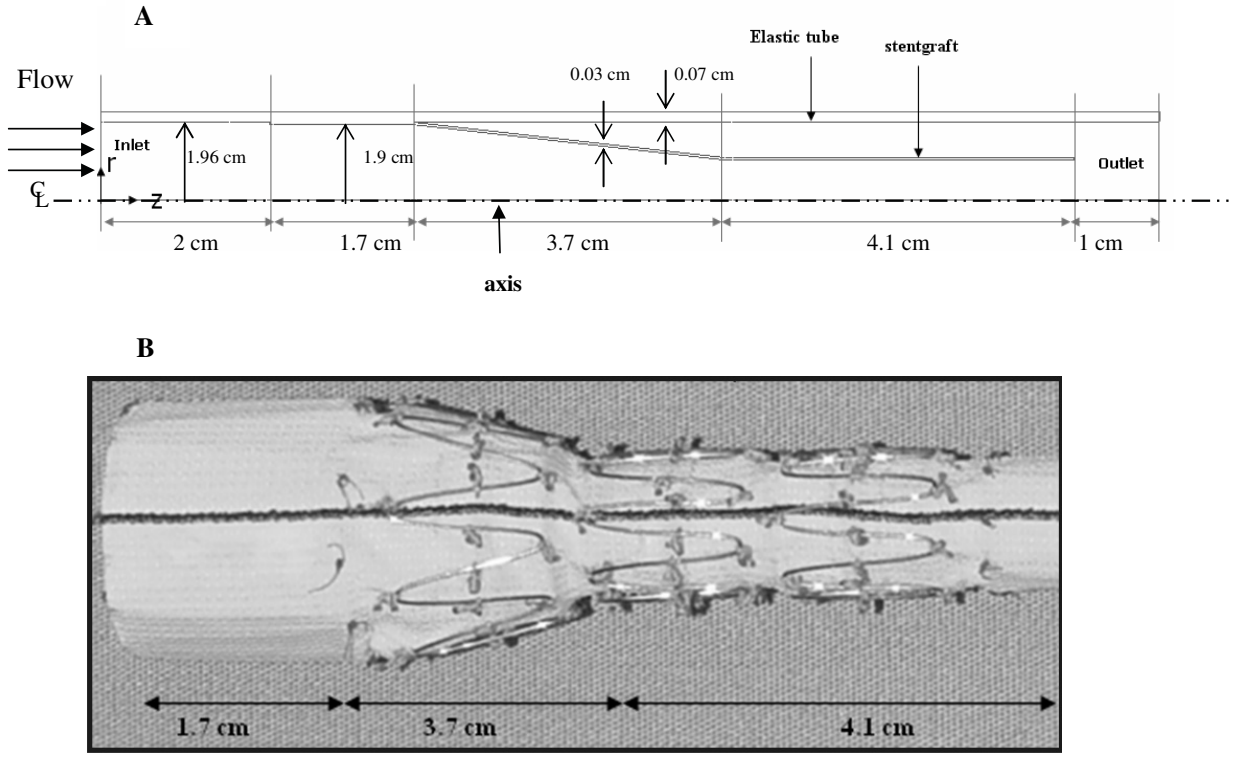

Figure 2: A. 2D axi-symmetric model; B. Stentgraft used for the *in vitro* experiment.

Table 1: Material properties for the elastic tube and stentgraft in the *in vitro* experimental study.

Parameters	Elastic Tube	Stentgraft
Wall thickness	0.07 cm	0.03 cm
Diameter (inner)	1.96 cm	Inlet -1.9 cm Outlet -1 cm
Young's modulus (E)	1.8MPa	10 GPa
Poisson ratio	0.49	0.27
Density	1.12 g/cm^3[8]	6 g/cm^3[8]

and inner stentgraft. The inner diameter of the stentgraft is d_i^s=1.9 cm at the inlet and d_o^s=1 cm at the outlet. The inner diameter of the outer elastic tube is d_i^e =1.96 cm with t^e= 0.07 cm thickness. The stentgraft is assumed to be isotropic with a uniform thickness of t^s=0.03 cm and attached to the inner wall of the elastic tube at the proximal end while the distal end is left free. Previous models of AAA stentgraft have distal portion of iliac limb attached to the iliac artery $d_i^s = d_o^s$[2-5]. The material properties of the stentgraft and the elastic tube used in the *in vitro* model are shown in the Table 1.

3.2 Governing Equations and Boundary conditions

3.2.1 Fluid Model

The fluid domain has been modeled as laminar, incompressible, homogenous and Newtonian. For large arteries such as the iliac artery, a Newtonian assumption for fluid is acceptable [22]. The arbitrary Lagrangian-Eulerian (ALE) formulation is used to solve the momentum and continuity equation of fluid flow. The *in vitro* data consists of flow rate, proximal and distal pressure. The pressure and flow data acquisitions were not performed simultaneously. Thus, the flow and pressure data

were not acquired with the same reference initial time, i.e., t = 0 was not the same for the acquired data. Moreover, the pressure was measured closer to inlet and outlet of the stentgraft whereas the flow rate was measured 60 cm proximal to the stentgraft. Hence, the inlet and outlet pressure wave have been imposed as boundary conditions as it results in reduced computational domain and time. In order to account for the phase difference and to obtain same reference time for the pressure and flow profile in the *in vitro* measurement, the following procedure is used:

1. First a flow computation for the model (Fig. 2A) without blood flow-compliant arterial wall interaction is performed with inlet boundary condition of flow rate and outlet pressure (p_o), which were obtained from the *in vitro* experiment.

2. The pressure at the inlet is obtained from the above computation. A phase shift of 0.027 sec between the calculated proximal pressure from the above step and experimentally obtained proximal pressure (p_i) is obtained. When this phase shifting was accounted for in the computational drag force data obtained from the above step, the time instant at which computational peak drag force was attained matched with the time instant at which the experimental peak drag force was attained.

3. Therefore for the blood flow-compliant artery wall interaction computation, the p_i is phase shifted by 0.027 sec and specified as normal traction at the inlet while p_o (without phase shifting) is specified as normal traction at the outlet.

The governing equations for the fluid domain are:

$$\rho(\frac{\partial u}{\partial t} + ((u-u_m).\nabla u) = -\nabla p + \nabla.(\mu \nabla u) \quad (1)$$

$$\nabla.u = 0 \quad (2)$$

where u is the velocity vector.

The boundary conditions used for the computations are:

$$\text{Pressure at the inlet} = p_i(t) \quad (3)$$

$$\text{Pressure at the outlet} = p_o(t) \quad (4)$$

$$u_r \text{ at the axis} = 0 \quad (5)$$

$$u_r \text{ at the inlet} = 0 \quad (6)$$

where u_m is the mesh velocity, u_r is the radial velocity and $u - u_m$ is the relative velocity of the fluid with respect to the moving coordinate velocity.

The drag force acting on the stentgraft along the z direction can be evaluated at each time t using eq. 7:

$$p_i a_i - p_o a_o + F_D = (\dot{m}_i \overline{u}_i - \dot{m}_o \overline{u}_o) + \frac{\partial}{\partial t} \int_v \rho u dv \quad (7)$$

where a = cross-sectional area, F_D = drag force, $\dot{m}$ = mass flow rate and v = complete volume of the fluid domain. The equation 7 shows the components of the drag force: the pressure force, shear stress along the stentgraft surface and inertia of the flowing blood. In the computations, the drag force has been obtained directly from the code, which does a balance of pressure force, shear and inertial force at each time along the stentgraft surface. Thus the drag computed numerically by the code would be the same as drag force computed if equation 7 had been used.

3.2.2 Solid model (Stentgraft and Elastic tube)

The stentgraft and the outer elastic tube is the solid domain which is assumed to be homogeneous, linear and isotropic. Table 1 lists the material properties of the stentgraft and the elastic tube. The governing equation and boundary condition for the elastic tube and stentgraft domain are as follows:

$$\sigma^S_{\alpha\beta,\beta} = 0 \quad (8)$$

$$d^S = d^F \quad (9)$$

$$\sigma^S_{\alpha\beta}.n_\beta = 0 \quad (10)$$

$$\sigma^S_{\alpha\beta}.n_\beta = \sigma^F_{\alpha\beta}.n_\beta \quad (11)$$

where d^S, d^F, $\sigma^S_{\alpha\beta}$ and $\sigma^F_{\alpha\beta}$ are the displacements and stress tensors for the solid and fluid, respectively, and n is a unit vector normal to the boundary. Displacements and stresses at the fluid solid

interface are given by eq. (9) and eq. (11). The axial displacements d_z^S and d_z^F are set to zero at both inlet and outlet for the model. The radial displacement of the axis is set to zero (Fig. 2).

In addition to validation of *in vitro* drag force, computations have been done to calculate the peak drag when *in vivo* velocity and pressure waveform [23] are imposed as boundary condition to the present model. The fluid properties used: μ = 0.04 Poise and ρ= 1.05 gm/cm^3 are similar to blood. The fluid is considered to be Newtonian which is acceptable for large arteries such as aorta [22]. *In vivo* drag force in actual physiological condition for this particular type of stentgraft geometry has been analyzed and discussed further in the results section.

4 Numerical method

The finite element method [24, 25, 26] is utilized for simultaneously solving the solid and the fluid equations. The mesh in the fluid zone consists of triangular axi-symmetric elements while solid zone consisted of bilinear quadrilateral elements. The sparse matrix solver based on Gaussian elimination was used for solving the governing equation. The number of nodes for the fluid and solid zones were 7500 and 1500, respectively. Mesh dependency has been confirmed till the variation in solution was less than 0.5%. Convergence criteria used for the fluid and solid degrees of freedom were 10^{-6} and 10^{-7}, respectively. The second order trapezoidal rule of time integration is used for both solid and fluid equations. Computations are carried out for three cycles. After the first cycle, no further change in the solution was observed. Hence, the data presented in this study are those of the second cycle of the computation.

5 Results

Pressure and flow rate data obtained from the *in vitro* model are shown in Fig. 3A. The proximal pressure data is phase shifted by 0.027 sec as discussed in the methodology section which is shown in the Fig. 3B. The peak pressure and mean flow rate obtained in the *in vitro* model are 150 mmHg and 0.97 l/min, respectively, which are comparable to the physiological condition [18].

5.1 Validation of the computational and in vitro drag force

Fig. 4 shows the comparison between the numerical drag force obtained from the compliant artery model and the experimental drag force measured by the load cell. The drag force is calculated along the stentgraft wall except where the stentgraft surface is attached to the outer elastic tube. The peak drag force obtained for the compliant artery model is 2.57 N and for the *in vitro* model it is 2.79 N; thus, a percentage difference of 7.8 % is observed. After 0.4 sec, fluctuations seen in the drag force data are mainly caused by wave reflection of pressure and flow from the downstream and upstream end reservoir or tank of the flow loop. These results provide the minimum fixation force necessary for the stentgraft to be in position after the intervention procedure.

5.2 Radial dilation of the outer elastic tube

Fig. 5A shows the specific location along the inner wall of the elastic tube where the deflections are reported. 1, 2, 3 and 4 are the locations along the inner wall of the elastic tube and points 5, 6 are the locations where the stentgraft is in contact with the silicon tube. Fig. 5B-C show the radial dilation of the elastic tube at specific location for one cycle. The initial radius at the inlet and outlet of the elastic tube is 0.98 cm. Since the outer elastic tube is compliant with E = 18 x 10^6 dynes/cm^2, the maximum and minimum radius of the elastic tube varied between 0.95 cm to 1.10 cm, respectively. The mean inlet and outlet radius of the elastic tube is 1.033 cm and 1.030 cm, respectively. The radial dilation at location 5 and 6 are minimal because the stentgraft is stiffer than the elastic tube which restricts the dilation. The stentgraft surface between locations 5 and 6 is the one which is attached to the iliac artery under *in vivo* condition.

5.3 Circumferential stress along the radial direction in the elastic tube

Figure 6A shows the circumferential stress at specific locations along the elastic tube and Fig. 6B

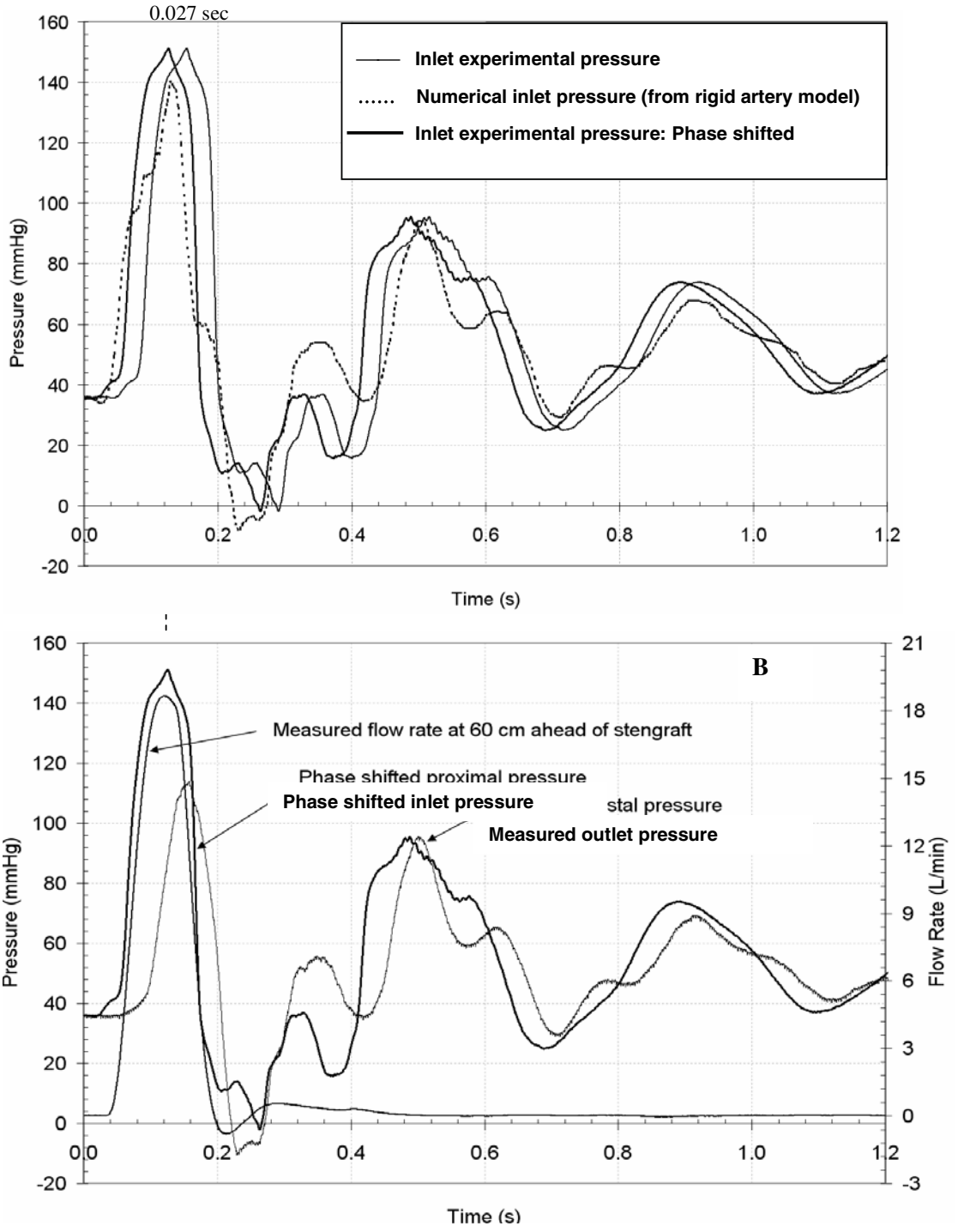

Figure 3: A. *In vitro* time varying proximal and distal pressure; B. Phase shifted time varying proximal pressure and flow rate.

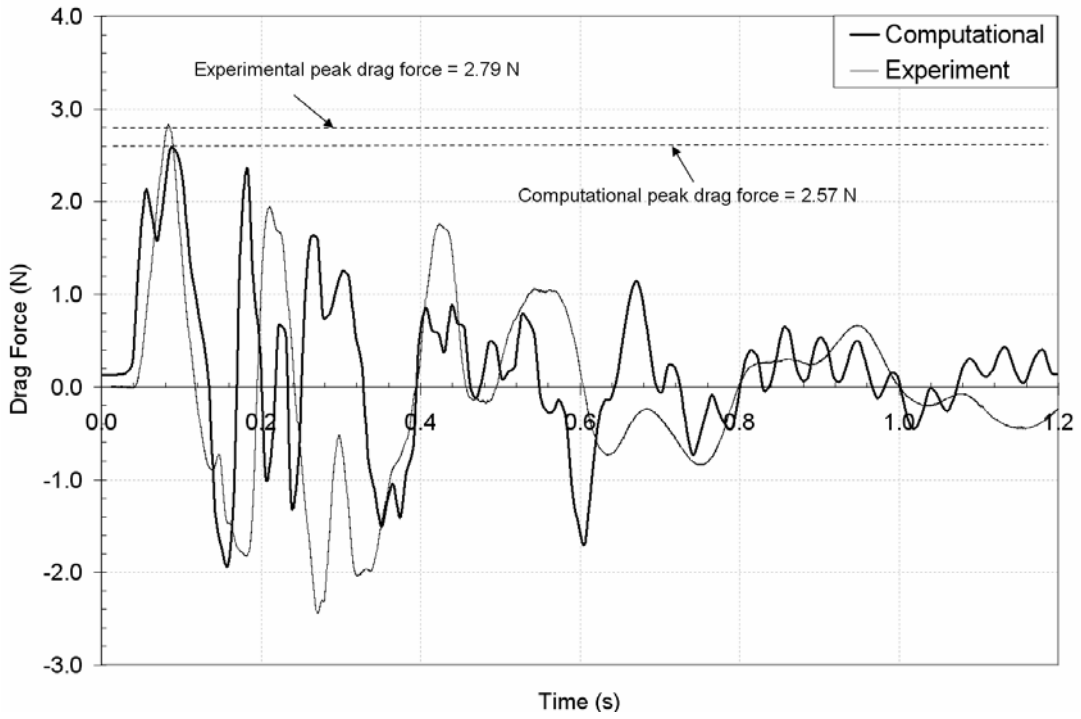

Figure 4: Comparison between experimental and numerical drag force.

compares the circumferential stress with time at locations 1, 2, 3, 4 at the middle of the elastic tube wall thickness. The peak circumferential stress of about 4 MPa is obtained at location 1 in the elastic tube, while the distal location 3 and 4 shows a peak stress of about 2.5 MPa. The mean stress at the inlet and outlet is about 1.18 MPa and 1.06 MPa, respectively.

5.4 Variation of the drag force along the stentgraft wall surface using in vivo pulse

Fig. 7A-C show the *in vivo* velocity and the pressure waveform used for simulating the actual physiological condition, respectively [22]. Fig. 7A and B show the *in vivo* velocity and pressure waveform of a typical abdominal aorta. The peak drag force is 0.59 N. Further, this configuration of the stentgraft is more effective for the *in vivo* set up than the *in vitro* model under dynamic physiological conditions.

6 Discussion

There are two types of stentgraft configurations available for treating abdominal aortic aneurysms: i) a bifurcated device, and ii) a aortouniiliac device. Both of these devices utilize main body extensions for the purpose of sealing the distal portion of the device within the iliac artery. Recently, Zenith® Renu™ AAA ancillary graft (Cook Incorporated, IN) has been approved by the Food and Drug Administration for salvage of previously placed endovascular prosthesis that have suffered migration or other events to the proximal fixation or sealing segments. If AAA's can effectively be treated by endovascular means, then repairing aneurysms involving internal iliac arteries, renal arteries, and the visceral vessels should be achievable by similar means. The architecture of the iliac limb stentgraft studied by the authors is comparable with a main body extension stentgraft. The need for secondary endovascular repair due to stentgraft migration can be reduced by using the proposed iliac limb stentgraft design in patients with abdominal aortic or aorto-

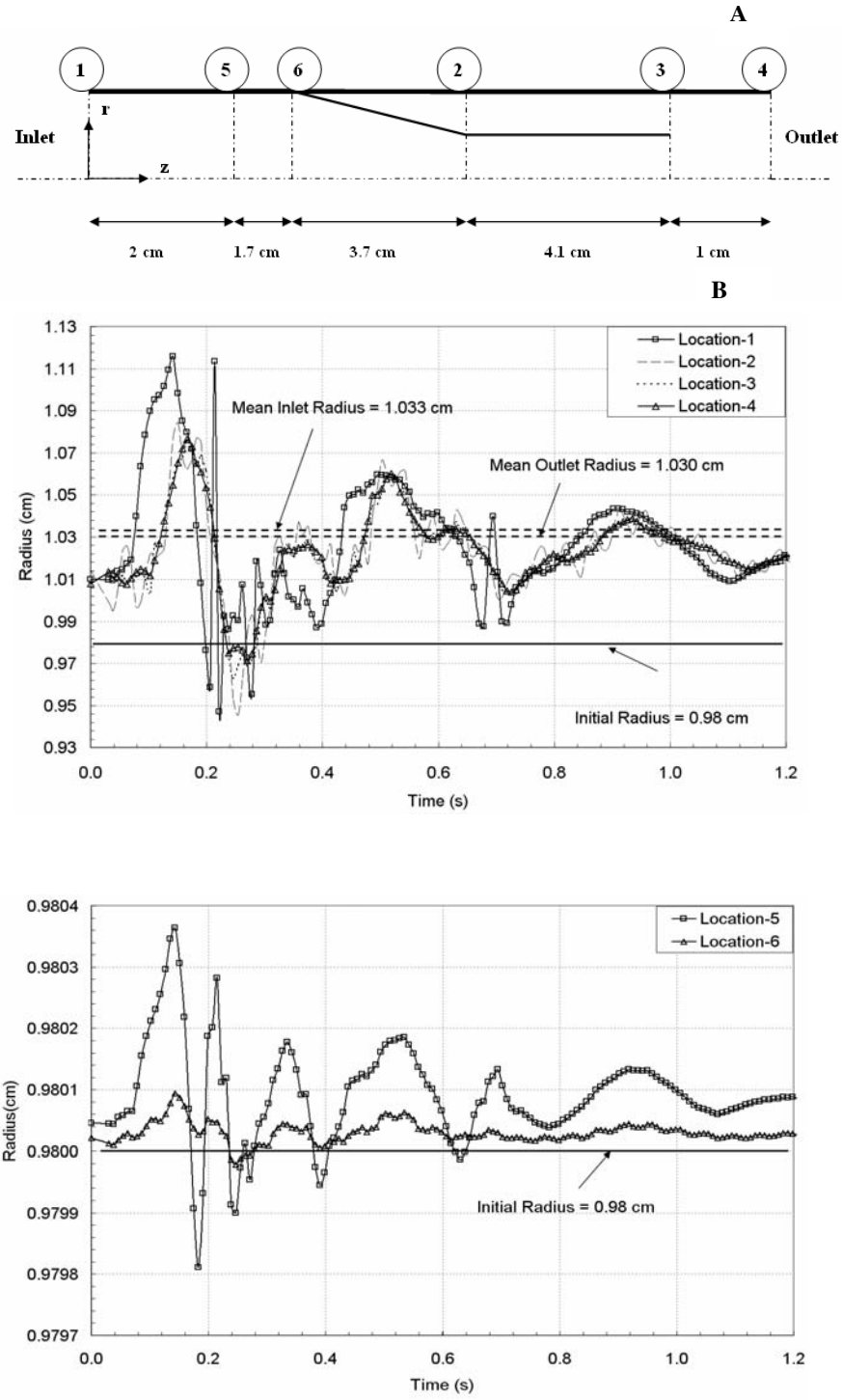

Figure 5: A. Specific location along the inner wall of the elastic tube where the deflections are reported; B & C Radial deformation at different locations

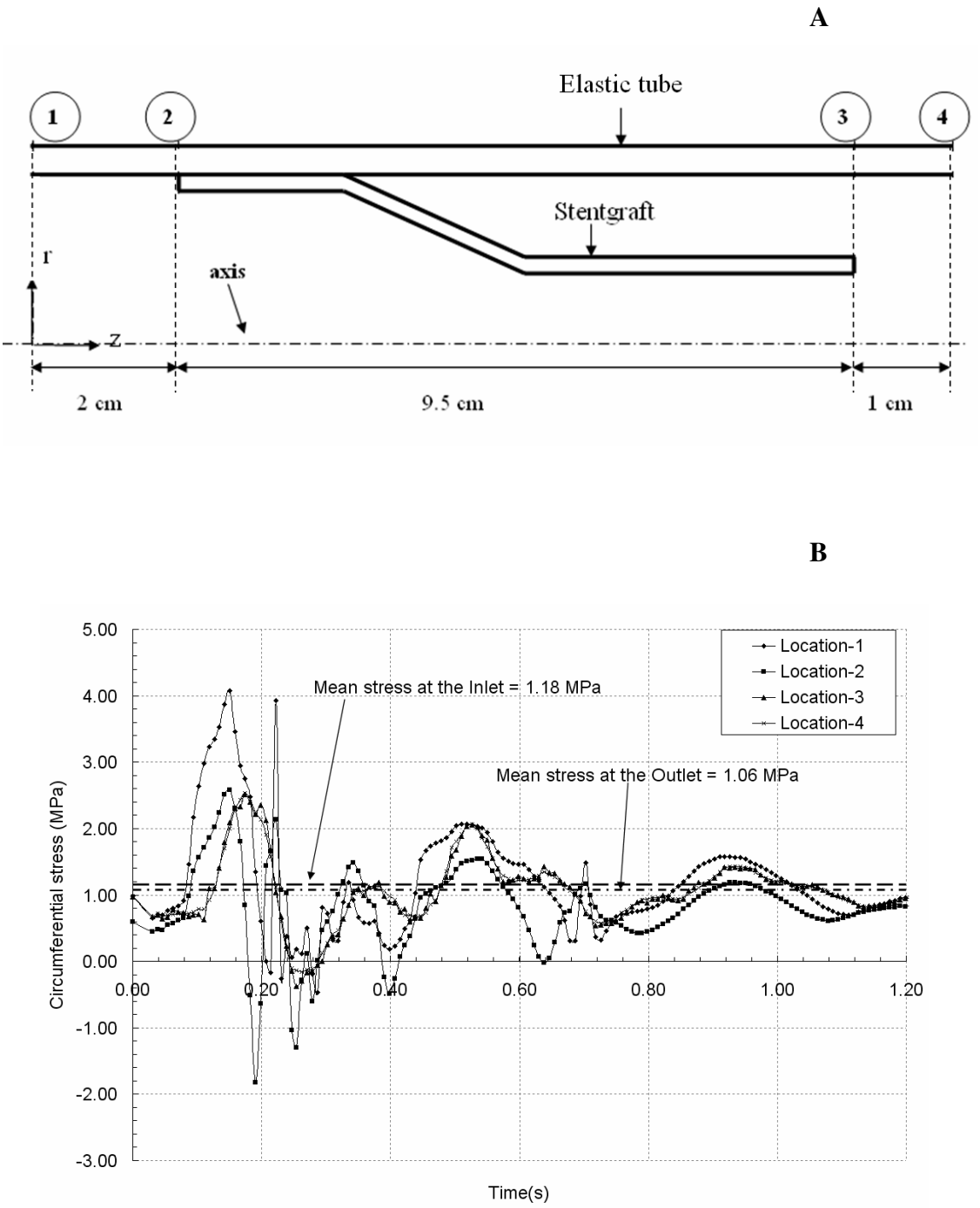

Figure 6: A. Specific locations along the elastic tube where the stress values are reported; B. Time varying circumferential stress along the elastic tube.

iliac aneurysms.

In previous studies [8-14, 30], the drag force was evaluated for the bifurcated AAA stentgraft that was fixed in the proximal end and distal limb diameter was the same as the iliac artery diameter. However, in this study only the iliac limb portion of the stentgraft was considered. The focus of the present study was to assess the variation of the

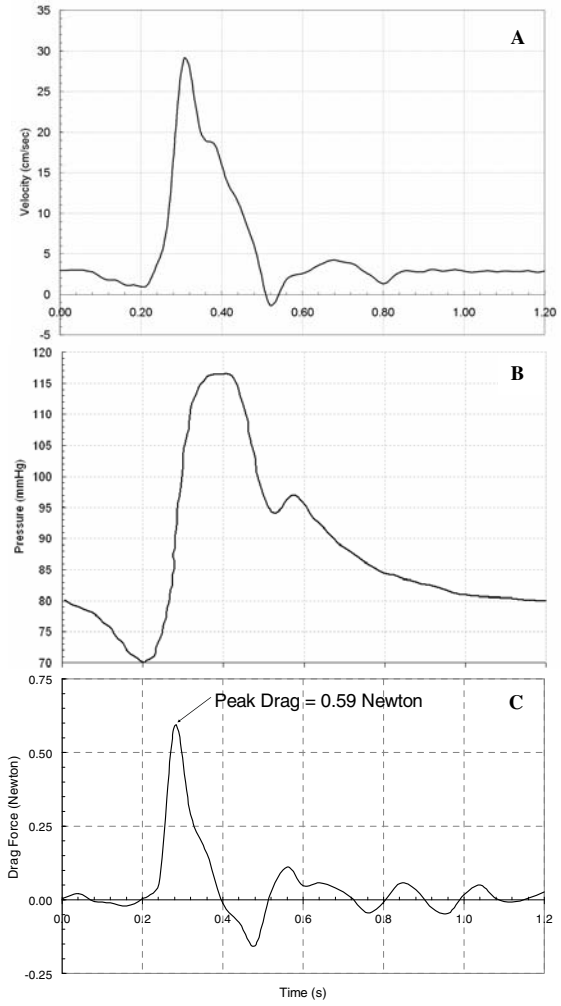

Figure 7: *In vivo* pulsatile velocity (A), pressure profile (B) and variation of pulsatile drag force (C) along stentgraft surface for the *in vivo* pulse.

drag force on the iliac limb stentgraft, by reducing the diameter of the distal end of the stentgraft and keeping it free. It was evident that when the distal end of the stentgraft, for the selected configuration (Fig. 1A; left limb of the bifurcation), was of same diameter as iliac artery, the outer surface of the stentgraft experienced a constant arterial sac pressure and higher net drag force. Hence, the drag force profile in the previous studies had similar trend as the pressure profile used in their model [8-11, 30]. In this study, the drag profile was different from the pressure profile (fig. 7C). This was due to the effect of pulsatile pressure acting on both the outer and inner surfaces of the stentgraft instead of constant sac pressure when the distal end of the stentgraft has a diameter equal to the diameter of the iliac artery. There is reduction in peak drag because of the increased annulus area between the distal sections of the artery and the stentgraft, which enhances the opposing drag force acting on the outer surface of the stentgraft and thus reducing the peak drag force on the complete system.

The possibility of utilizing particular physiological conditions to increase the stability of stentgrafts is important. At the present time, several design concepts that could possibly benefit from the presented geometry are being investigated. For example, the stent-graft geometry illustrated in figure 1 is an abdominal aortic aneurysm that can also be repaired by using an aortomonoiliac device and cross-femoral bypass grafting. As the pressure within the aneurysm sac decreases post implantation, the tapered graft's hemodynamic forces want to displace the stent-graft into the aneurysm sac causing a Type III leak. Since the number of stent-graft components are subject to increase, the number of modular joints and the risk of Type III leaks (component separation and/or stent-graft migration) are also subject to increase. A possible solution to this problem would be to allow a decreased level of systemic pressure to exist within the sac offsetting the pressure difference and decreasing the probability of stent-graft migration. This analogy can be applied to the development of branch vessel devices aiding in reducing hemodynamic displacement forces. For example, if the sac pressure were 50% of the systemic pressure, theoretically, the hemodynamic displacement forces would also be reduced by 50% (this would be neglecting drag and gravitational forces). There are several issues that would need to be addressed in applying this technology, one being the possibility of the transmural pressure contributing to the continued growth of the aneurysm. Therefore further studies would need to be completed to determine an acceptable sac pressure.

The inlet and outlet diameters of the iliac limb of bifurcated stentgraft in previous models [8-11] are

1.7 cm and 1.1 cm respectively, which are comparable to the diameters of 1.9 cm and 1 cm respectively, used in this study. Past studies [27-29] have concentrated more on the stress patterns in the abdominal aneurysm before and after stentgraft placement and concluded that the stentgraft reduces the wall shear stress in the aneurysm by 85%. Thus, this study demonstrates reduction in the drag force due to the opposing forces acting on the outer cavity region of the stentgraft. The limitation of this study is that the flow and pressure data for the *in vitro* model have not been set to produce the *in vivo* flow and pressure waveforms. Improvements in the data acquisition, such as simultaneous triggering of pressure and flow probes; thus fixing a unique start time for data acquisition, can enable us to avoid estimation of phase shifting by computational means.

The elastic tube along with the stentgraft is immersed in a water bath at a depth of approximately 1.5 cm. The pressure head produced by 1.5 cm depth of water is negligible in comparison to level of pressure inside the elastic tube. Anisotropic behavior of the artery was not considered. Rather a linear isotropic behavior was used for the elastic tube. However, the stentgraft consists of metallic stents woven onto a graft which reduces its compliance significantly (order of E $\sim 10^{10}$ dynes/cm^2). Hence the additional reduction in compliance in the computational model due to stents should not produce significant change in flow dynamics of the stentgraft for the blood flow-compliant artery wall analysis and the assumption of homogeneous material for the stentgraft is valid for this study. In future, the in vivo calculations could be performed with hyperelastic incompressible arterial material properties [31] for better estimation of drag. Clinical issues like thrombus formation and cellular interaction [32], decrease in the wall shear stress due to reverse flow seen at the distal end of the stentgraft and optimization of stentgraft distal diameter will need further investigation.

In summary, this study investigates the peak drag force on the iliac limb section of the stentgraft that is downstream the bifurcated abdominal aortic stentgraft. The selected design reduces the drag force considerably when used in the actual dynamic physiological conditions. This study investigates the drag force by both computational and experimental means and provides insights into the hemodynamic parameters of the stentgraft. Additional investigation like optimal iliac limb diameter with respect to the distal artery diameter in conjunction with the entire bifurcated stentgraft design and improved *in vitro* experiment to simulate the exact physiological pulse are considered for the future work.

Nomenclature

u	velocity
p	pressure
$\overline{u}$	average velocity
d	diameter
r	radius
t	time
E	Young's modulus

Superscripts

S	solid
F	fluid
s	stentgraft
e	elastic tube

Subscripts

z	axial
r	radial
θ	circumferential
α, β	co-ordinate directions
i	inlet
o	outlet

References

1. Pierre Monney, Daniel Hayoz, Francine Tinguely. High prevalence of unsuspected abdominal aortic aneurysms in patients hospitalised for surgical coronary revascularization. European Journal of Cardio-thoracic Surgery 2004; 25:1.

2. Endovascular aneurysm repair versus open repair in patients with abdominal aortic

aneurysm (EVAR trial 1): randomized controlled trial. Lancet 2005; 365(9478):2179-2186.

3. Greenberg RK, Chuter TA, Sternbergh WC, III, Fearnot NE. Zenith AAA endovascular graft: intermediate-term results of the US multicenter trial. J Vasc Surg 2004; 39(6):1209-1218.

4. Matsumura J, Brewster D, Makaroun M, Naftel D. A multicenter controlled clinical trial of open versus endovascular treatment of abdominal aortic aneurysm. J Vascular Surgery 2003; 37(2):262-271.

5. Beebe HG. Lessons learned from aortic aneurysm stent graft failure; observations from several perspectives. Semin Vasc Surg 2003; 16(2):129-138.

6. Jacobs TS, Won J, Gravereaux EC, Faries PL, Morrissey N, Teodorescu VJ et al. Mechanical failure of prosthetic human implants: a 10-year experience with aortic stent graft devices. J Vasc Surg 2003; 37(1):16-26.

7. Greenberg RK, Turc A, Haulon S, Srivastava SD, Sarac TP, O'Hara PJ et al. Stent-graft migration: a reappraisal of analysis methods and proposed revised definition. J Endovasc Ther 2004; 11(4): 353-363.

8. Li Z, Kleinstreuer C. Fluid–structure interaction effects on sac-blood pressure and wall stress in a stented aneurysm. J Biomechanical Engineering (ASME) 2005; 127:662–671.

9. Li Z, Kleinstreuer C. Analysis of biomechanical factors affecting stent-graft migration in an abdominal aortic aneurysm model. J Biomechanics. In press

10. Li Z. Computational fluid–structure-interaction analyses applied to stented aneurysms. Ph.D. Thesis, MAE Department, NC State University, Raleigh, NC, USA, 2005

11. Li Z, Kleinstreuer C. Blood flow and structure interactions in a stented abdominal aortic aneurysm model. Medical Engineering & Physics 2005;27:369–382.

12. Morris L, Delassus P, Walsh M, McGloughlin T. A mathematical model to predict the *in-vivo* pulsatile drag forces acting on bifurcated stent grafts used in endovascular treatment of abdominal aortic aneurysms (AAA). J Biomechanics 2004;37: 1087–1095

13. Liffman K, Lawrence M, Semmens B, Bui A, Rudman M, Hartley D. Analytical modeling and numerical simulation of forces in an endoluminal graft. J Endovascular Therapy 2001; 8:358–371.

14. Di Martino ES, Guadagni G, Fumero A, Ballerini G, Spirito R, Biglioli P, Redaelli A. Fluid–structure interaction within realistic three-dimensional models of the aneurysmatic aorta as a guidance to assess the risk of rupture of the aneurysm. Medical Engineering Physics 2001;23:647–655

15. Chong CK, How TV. Flow patterns in an endovascular stent-graft for abdominal aortic aneurysm repair. J Biomechanics 2004; 37:89–97

16. Volodos SM, Sayers RD, Gostelow J.P, Bell P. Factors affecting the displacement force exerted on a stent graft after AAA repair—an *in vitro* study. European Journal of Vascular and Endovascular Surgery 2003; 26: 596–601.

17. Lambert AW, Williams DJ, Budd JS, Horrocks M. Experimental assessment of proximal stent-graft (IntervascularTM) fixation in human cadaveric infrarenal aortas. European Journal of Endovascular Surgery 1998; 17:60–65.

18. Malina M, Lindblad B, Ivancev K. Endovascular AAA exclusion: Will stents with hooks and barbs prevent stent-graft migration?. J Endovascular Surgery 1998; 5: 310–317.

19. Lawrence Leigh, Dmitry Rabkin, Kevin Berbaum, Thomas G. Vrachliotis, David P.Brophy, Elvira V. Lang. Impact of graft material configuration on stent-graft endoleaks *in vitro*. J Vascular Interventional Radiology 2001; 12:1423-1427

20. Resch T, Malina M, Lindblad B, Malina J, Brunkwall J, Ivancev K. The impact of stent design on proximal stentgraft fixation in the abdominal aorta: an experimental study. European Journal of Endovascular Surgery 2000; 20:190–195.

21. Resch T, Malina M, Lindblad B, Malina J, Brunkwall J, Ivancev K. Distal migration of stent-grafts after endovascular repair of abdominal aortic aneurysm. J Vascular Interventional Radiology 1990; 10:257-264.

22. Pertold K, Resch M, Florian H. Pulsatile non-Newtonian flow characteristics in a three dimensional human carotid bifurcation model. J Biomech Eng 1991; 113:464-75.

23. Christine MS, Alexander DS, Satish CM, Finol A. Fluid-structure interaction in abdominal aortic aneurysm: effects of asymmetry and wall thickness. Biomedical Engineering Online. 2005; 4:64.

24. ADINA. Theory and modeling guide, Vols. I & III 2004. Watertown, MA

25. Bathe KJ, Zhang H, Ji S. Finite Element Analysis of Fluid Flows Fully Coupled with Structural Interactions. Computers & Structures 1999; 72: 1-16.

26. Bathe KJ, Zhang H. Finite Element Developments for General Fluid Flows with Structural Interactions. Int. Journal for Numerical Methods in Engineering. 2004; 60: 213-232, 2004.

27. Di Martino ES, Bohra A, Scotti CM, Finol EA, Vorp DA. Wall Stresses Before and After Endovascular Repair of Abdominal Aortic Aneurysms. AAA Pre- and Post-EVAR, IMECE2004-61556. ASME IMECE: Bioengineering 2004 Anaheim, CA, USA.

28. Scotti, C.M., Finol, E.A., Viswanathan, S., Shkolnik, A., Amon, C.H., Vorp, D.A., Di Martino, E., 2004. Computational fluid dynamics and solid mechanics analyses of a patient-specific AAA pre- and post-EVAR (IMECE2004-62352). ASME IMECE: Bioengineering, Anaheim, CA, USA

29. Thubrikar M, Al-Soudi J, Robicsek F. Wall stress studies of abdominal aortic aneurysm in a clinical model. Annals of Vascular Surgery 2001; 3:355–366.

30. Scotti MC, Cornejo SL, Finol EA. Biomechanics of Abdominal Aortic Aneurysms: Flow-Induced Wall Stress Distribution. ICCES, 2007; 1, 41-48.

31. Fung, YC, Tong P, Classical and Computational Solid Mechanics, World Publishing Company, 2001.

32. Kurpinski K, Park J, Thakar RG, Li S. Regulation of Vascular Smooth Muscle Cells and Mesenchymal Stem Cells by Mechanical Strain. Mol Cell Biol. 2006; 3: 21-34.